

Article

Integration of Carboxymethyl Cellulose Isolated from Oil Palm Empty Fruit Bunch Waste into Bismuth Ferrite as Photocatalyst for Effective Anionic Dyes Degradation

Siti Aqilah Husna Md Azman ¹, Suresh Sagadevan ², Ishak Ahmad ³, Mohamad Haafiz Mohamad Kassim ⁴, Saifullahi Shehu Imam ⁵, Khoa Dang Nguyen ^{6,*} and Noor Haida Mohd Kaus ^{1,*}

¹ School of Chemical Sciences, Universiti Sains Malaysia, Penang 11800, Malaysia

² Nanotechnology & Catalysis Research Centre, University of Malaya, Kuala Lumpur 50603, Malaysia

³ Faculty of Science and Technology, School of Chemical Sciences and Food Technology, Universiti Kebangsaan Malaysia, Bangi 43600, Malaysia

⁴ School of Industrial Technology, Universiti Sains Malaysia, Penang 11800, Malaysia

⁵ Department of Pure and Industrial Chemistry, Bayero University, Kano P.M.B 3011, Nigeria

⁶ Faculty of Environment, School of Engineering and Technology, Van Lang University, Ho Chi Minh 700000, Vietnam

* Correspondence: khoa.nd@vlu.edu.vn (K.D.N.); noorhaida@usm.my (N.H.M.K.)



Citation: Md Azman, S.A.H.; Sagadevan, S.; Ahmad, I.; Kassim, M.H.M.; Imam, S.S.; Nguyen, K.D.; Kaus, N.H.M. Integration of Carboxymethyl Cellulose Isolated from Oil Palm Empty Fruit Bunch Waste into Bismuth Ferrite as Photocatalyst for Effective Anionic Dyes Degradation. *Catalysts* **2022**, *12*, 1205. <https://doi.org/10.3390/catal12101205>

Academic Editors: Krzysztof Miecznikowski and Beata Krasnodębska-Ostrega

Received: 13 September 2022

Accepted: 8 October 2022

Published: 10 October 2022

Publisher's Note: MDPI stays neutral with regard to jurisdictional claims in published maps and institutional affiliations.



Copyright: © 2022 by the authors. Licensee MDPI, Basel, Switzerland. This article is an open access article distributed under the terms and conditions of the Creative Commons Attribution (CC BY) license (<https://creativecommons.org/licenses/by/4.0/>).

Abstract: Photocatalytic biomass valorization has proven to be a valuable approach for sustainably constructing value—added products from waste materials. The present study aimed to know about Bismuth ferrite (BiFeO₃) nanoparticles combined into carboxymethyl cellulose (CMC) obtained from oil palm empty fruit bunch waste (OCMC) and used as a catalyst composite for the degradation of anionic dyes, specifically on methyl orange (MO) and congo red (CR). The parameter that affects the formation of OCMC, such as the degree of substitution (DS), depends upon the alkalization reaction time and NaOH concentrations. The highest DS was obtained at 1.562 and found at 60% NaOH with 9 h of alkalization, very close to that of the commercial CMC (CCMC) DS value. X-ray diffraction (XRD) analysis revealed that OCMC as a semi-crystalline phase and the tensile strength of OCMC film increased significantly from 0.11 MPa to 3.54 MPa as compared to CCMC. The comparative study on photocatalytic degradation of MO and CR using OCMC and CCMC reinforced with 0.8% BiFeO₃ showed a minor difference in removal percentage. The efficiency removal for CCMC/BFO towards CR and MO was enhanced to 95.49% and 92.93% after a 3-h treatment, and a similar result was obtained in the case of OCMC/BiFeO₃ at 92.50% for CR and 89.56% for MO, respectively. Nevertheless, it is interesting that OCMC film exhibits remarkable stability with an improvement in terms of tensile strength and stays more intact than that of CCMC.

Keywords: photocatalysis; nanoporous; materials; photo functional materials; biomass; OPEFB

1. Introduction

Nowadays, environmental pollutions are the major problem affecting the earth. The primary sources of this type of pollution are the excretion of industrial wastes and effluents. It might be in the form of solid waste, liquid waste, or gaseous waste. Enormous environmental contaminants discharged from textile and papermaking industries are non-biodegradable dyes and carcinogenic contaminants. Water pollution caused by various industries, including fertilizer, dyes, and other chemicals, is a significant concern on a global scale [1,2]. About one million tons of dyes are generated annually for consumption in the textile, leather, pharmaceuticals, paper, and cosmetic industries [1], and during the industrial processes, a huge amount of the dyes are released into effluents [3]. Unfortunately, these dyes are hazardous to the environment and non-biodegradable [4]; consequently, it is essential to have a proper approach for the removal of dangerous chemicals from water supplies [5]. Photocatalytic degradation utilizing semiconductors made up of metal-oxide

is an established approach for removing wastewater pollutants, including synthetic dyes [5]. The procedure is affordable, efficient, eco-friendly, and economical for the environment [6]. Heterogeneous photocatalysis reactions occur mostly on the photon-activated photocatalyst materials surface [7–9]. It is essential to understand the reaction steps involved in the photodegradation of organics when formulating kinetic expressions. The liquid phase organic compounds are degraded to their corresponding intermediates with increasing irradiation time and further mineralized to carbon dioxide, water, and inorganic ions (from heteroatoms) [10]. Among them, BiFeO₃ (BFO) has a narrower (~2.5 eV) band gap that allows the photocatalytic activity to become prominent under visible light. The smaller band gap of BFO nanoparticles indicates the possibility of photocatalysis using more visible light [11]. Therefore, applications of BFO materials either in pollutant degradation or in photocatalytic hydrogen generation from water splitting under visible light have attracted more attention [12]. According to Gao et al., BFO nanoparticles with the size of ~120 nm has been used to degrade methyl orange (MO) under visible light and after 16 h, almost all of the MO has been degraded [11]. The experiment of Xu et al. proved that BFO could degrade Congo red, albeit the effect of degradation is not as good [7]. These results predict that BFO may have the potential for effective water treatment applications [13]. However, due to their limited specific surface area and low adsorption capacity, the performance of conventional semiconductors is insufficient to satisfy the demands of actual applications. Photocatalyst removal or recovery work with suspensions is not technically feasible due to the high cost of the filtration process. When added to fixed beds or other flow-through systems, the reduced particle size and potential leaching of these photocatalyst nanoparticles may hinder mass movement and result in the excessive pressure reductions [13]. In addition to issues with separation and reuse, nanoparticles released into the environment could pose risks to ecosystems and human health. To get over these restrictions, a workable method is to build a hybrid nanocomposite by impregnating or immobilizing the small particles on bigger solid particles. The photocatalyst and adsorbents are joined to form an integrated photocatalyst adsorbent. For enriching organic molecules on photocatalyst surfaces for catalytic conversion, these porous/composite materials seemed to be a preferable choice.

Biomass waste, particularly from the oil palm empty fruit bunch (OPEFB), has generated more than 18,000 tonnes; cellulose extracted from OPEFB has been determined to be 93% pure [14]. OPEFB biomass waste has low economic value and poses a disposal challenge most of the time. Conventionally, OPEFB waste is often burnt, disposed of in landfills, or composted with organic fertilizer [15,16]. As a result, solid waste such as OPEFB pulp is available and can be transformed into a low-viscosity cellulose-based product, resulting in the better utilization of biological resources, less pollution, and significant economic and environmental advantages.

Carboxymethyl cellulose (CMC) is a linear, long-chain, water-soluble, anionic polysaccharide and is one of the most valuable and important derivatives of cellulose. It has been known as a promising polymer adsorbent with high porosity, viscosity, non-toxicity, and biodegradability [17]. CMC is prepared by activation of cellulose with an aqueous NaOH in the slurry of an organic solvent which reacts with the cellulose and monochloroacetic acid (MCA) as an etherifying agent [18–20]. As a result, hydroxyl groups are substituted by sodium carboxymethyl groups in C-2, C-3, and C-6 of glucose, and substitution slightly prevails at the C-2 position [21]. Hence, the substitution of a carboxymethyl group instead of the hydroxyl groups is slightly predominant at the C-2 glucose position [18]. Through this reaction, different degrees of substitution (DS) of CMC, a key property affecting the physical and chemical properties of CMC for many applications, can be produced generally in the range of 0.5–1.4 for commercial products [22]. Although the maximum theoretical value of substitution is 3, this value reached up to 1.4 for commercially available ones. The CMC with DS < 0.4 swelled but was insoluble in water, while the CMC with a DS of more than 0.4 was fully soluble with its hydro-affinity, which increases with the rise of DS [23]. It was discovered that the DS increases significantly with temperature and time; however, the effect of time on DS is greater than that of temperature [24]. Due to the

degradation of CMC under the influence of atmospheric oxygen, the DS value decreased with a further increase in reaction temperature. This is because the long reaction time improves diffusion and absorption of the reagents, with the ultimate effect of improving contact between the etherifying agents and cellulose [25,26]. In addition, it was reported that increasing the concentration of NaOH had a greater impact on DS than increasing the temperature or SCA [27]. Since it is extensively employed in numerous areas, many studies have been conducted to produce CMC from different resources, such as sugarcane bagasse [21], durian rind [28], cornstalk [19], and palm kernel cake [29]. It was observed that the properties of the prepared CMC from various biomass sources have been attributed to the dose dependence of different factors. The suitable ratio of cellulose/SCA was noted at 5/6 (wt%) and a reaction time of 3 h [18,30–33]. In addition to this, the reaction temperature should be controlled, as DS decreased due to the degradation of CMC under the influence of atmospheric oxygen. However, as mentioned previously, the concentration of NaOH solution and reaction time was able to vary in a wide range depending on the biomass source. A higher concentration of NaOH might lead to the formation of the by-products in the side reaction, such as sodium chloride and glycolate, which reduced the purity of CMC [22]. However, Pinto et al. reported that the DS value could be achieved by using a higher concentration of NaOH solution [19].

Therefore, the present study uses a variety of alkalization times and NaOH concentrations to produce a hydrophilic, negatively charged CMC from OPEFB at lower reaction temperatures. The study has attempted to identify the polymer's best DS and mechanical properties before integrating it with the BiFeO₃ (BFO) semiconductor. It also investigated how well synthesized CMC associated with BFO (SCMC/BFO) degraded the dyes methyl orange (MO) and congo red (CR) through photocatalysis.

2. Results and Discussion

2.1. The Appearance of Cellulose Extracted from OPEFB, OCMC, and BFO Composite Films

Figure 1 shows the images of the OPEFB after pulping processes (a), the isolated cellulose from OPEFB (b), and the prepared CMC (OCMC) after 9 h reaction at 60% NaOH solution (c). It can be seen that the chemical treatment in the cellulose extraction process and carboxymethylation have strong effects on the formation of the obtained materials. After the alkalization and bleaching step, the initial pulped OPEFB was decolorized from a yellow–brown to a white color, as observed in the case of purified cellulose. In addition, the preparation of the OCMC necessitated two reactions: alkalization and etherification, respectively. The cellulose from OPEFB waste is alkalized with NaOH in the presence of isopropanol, which acts as a swelling agent and diluent, allowing effective penetration into the crystalline cellulose structure. It allows the hydroxyl groups to participate in the etherification reaction by solvating them, which was carried out at room temperature. To produce carboxymethyl cellulose ethers, alkali cellulose is reacted with MCA throughout etherifying isopropanol as the supporting medium. From these results, it could be suspected that the morphologies of the OCMC varied when different concentrations and reaction times of NaOH solutions were used. In addition, there was no significant difference between the films prepared from OCMC and CCMC as well as the nanocomposite materials of BFO in Figure 1d–g.

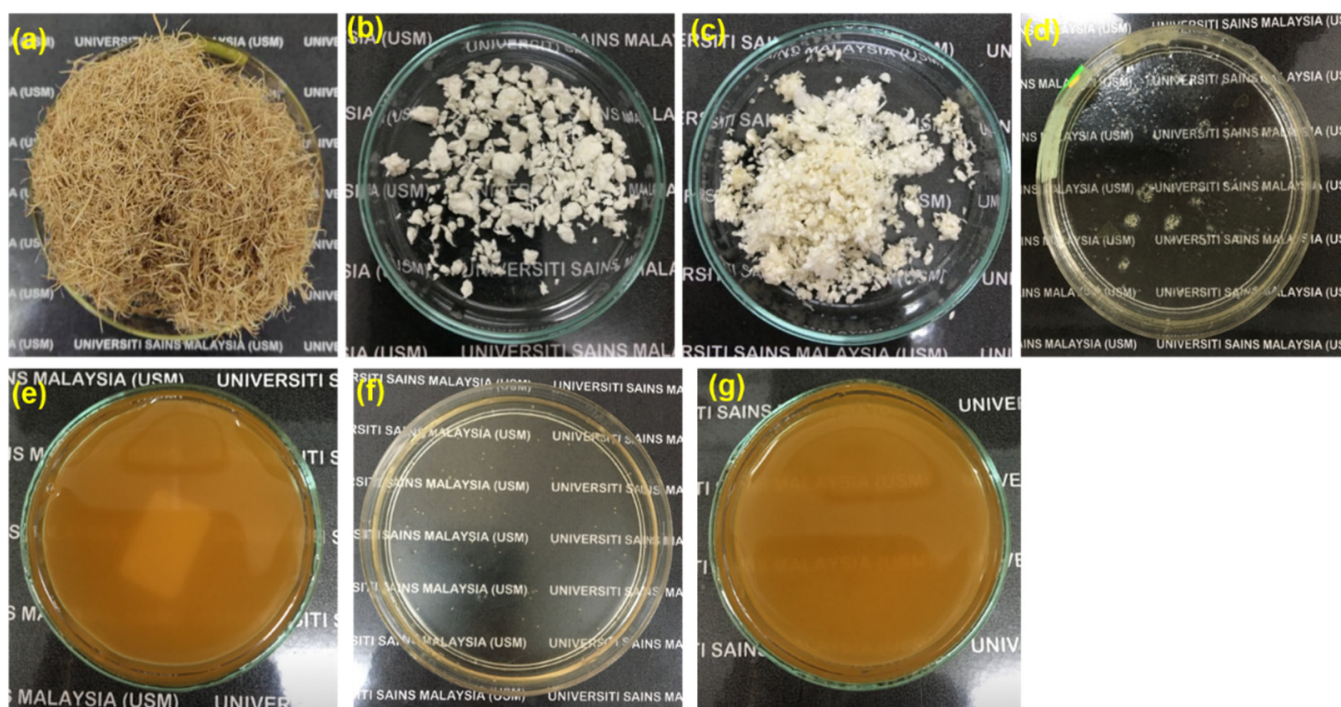


Figure 1. The appearance of pulped OPEFB (a), extracted cellulose from the pulped OPEFB (b), OCMC (c), films of OCMC (d), and OCMC/BFO (e); CCMC (f) and CCMC/BFO (g).

2.2. Effect of Various Alkalinization Times and Concentrations of NaOH towards the Degree of Substitution (DS)

The polymer's functional group's degree of substitution (DS) is an essential parameter. The average number of hydroxyl groups in the structure of cellulose that were substituted is the degree of substitution (DS) of the carboxyl group in CMC at C-2,3 and 6 by carboxymethyl groups. The DS of the OCMC was determined by synthesizing cellulose from OPEFB with different NaOH concentrations and alkalinization reaction times. The duration of alkalinization was investigated by varying the alkalinization period from 3 to 11 h while using 30% NaOH, and the degree of substitution (DS) was shown in Figure 2a. As can be seen, the DS of OCMC increased with increasing alkalinization time, and reached a maximum value of 0.688 after 9 h. This could be related to the formation of an alkali-cellulose slurry at longer the alkalinization reaction time and the cellulose reacted with NaOH, resulting in a more slurry-like combination. Monochloroacetate functional groups were thus actively encouraged to penetrate deeply into the crystalline cellulose structure. Above 9 h, the DS of OCMC tended to be decreased to 0.604 in 11 h. As the alkalinization period extended, the crystalline structure is disintegrated or altered, resulting in the decreasing DS [34]. It is noted that, for various cellulose sources, the distinct influence of NaOH concentration in the alkalinization stage on the subsequent etherification reaction and in conjunction with polymer swelling and cellulose crystallinity has been intensively highlighted [35]. As shown in Figure 2b, the effect of sodium hydroxide concentration was investigated by varying the NaOH solution concentration from 20 to 70%. The DS of OCMC increased with NaOH, reaching a maximum DS of 1.562 at a 60% NaOH in concentration. OCMC's capacity to sequester water in a system has improved as its DS has improved, attributable to its hydrophilicity toward liquids. When more than 60% alkali was utilized, the DS decreased to 0.781 when produced at 70% NaOH solution. The DS has reduced above 60% NaOH concentration, most likely due to cellulose breakdown and glycolate formation, resulting in the inactivation of MCA used by this side process [25]. In conclusion, the highest degree of substitution output was produced by an alkalinization process lasting 9 h with 60% NaOH, as shown in Figure 2a,b and this composition has continued for further use.

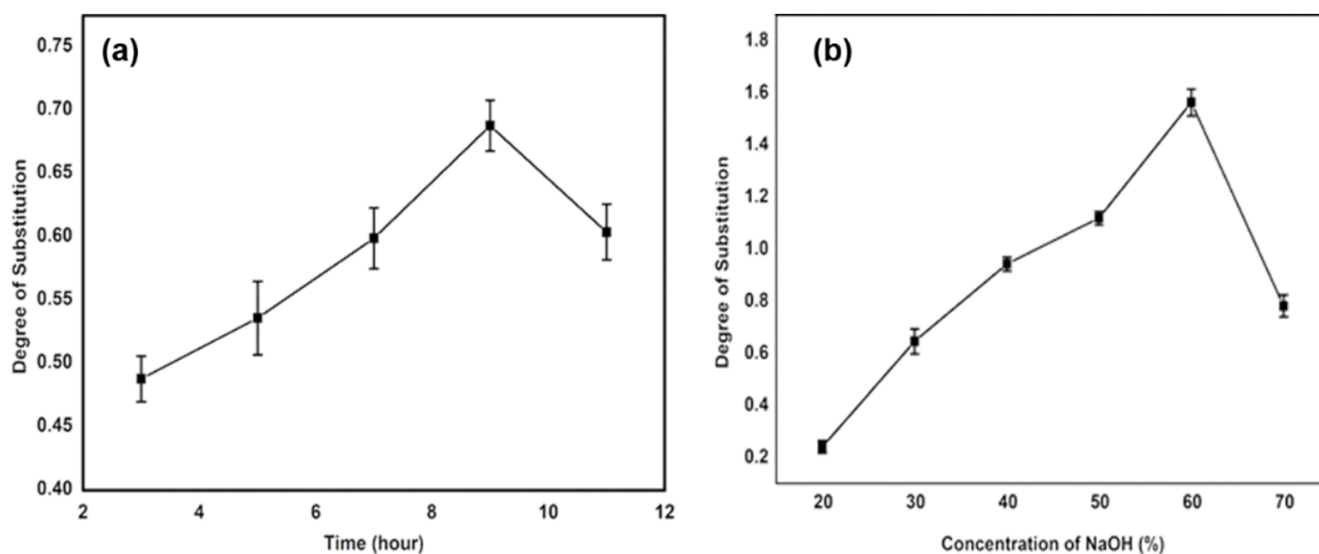
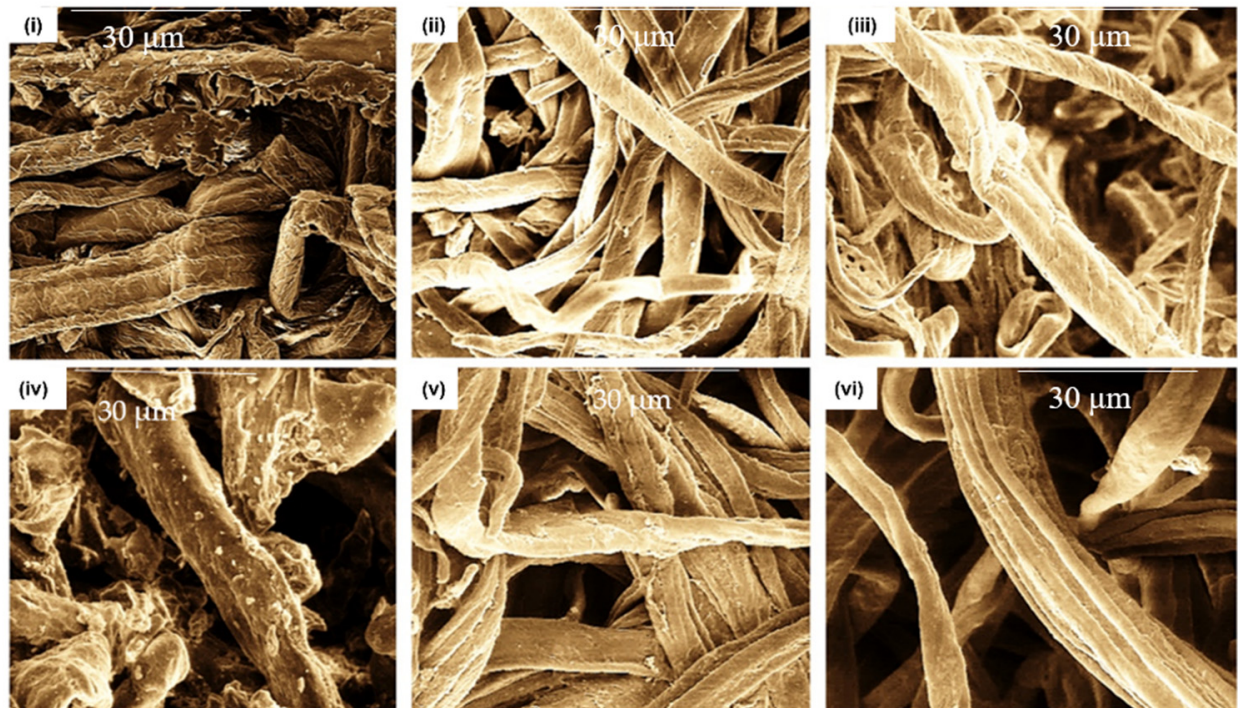


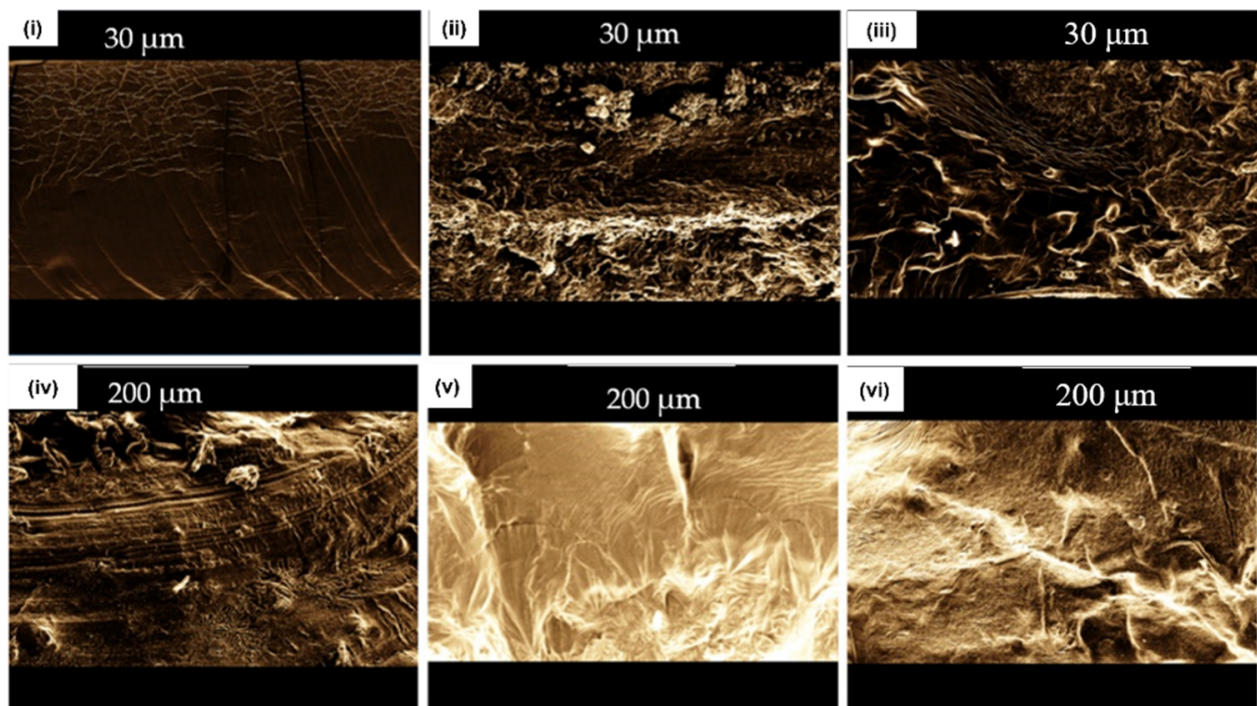
Figure 2. Effect of alkalization time on DS of OCMC in the presence of 30% NaOH (a) and Effect of NaOH concentration on DS of OCMC produced within 9 h (b).

2.3. Microstructure and Morphology

The control cellulose produced from OPEFB exhibited a rough exterior surface, and the fiber was twisted and ruptured, which was possibly caused by the employment of highly concentrated chemicals and high temperatures in the cellulose extraction process (Figure 3ai). The synthetic commercial carboxymethyl cellulose (CCMC) had a long and narrow form (Figure 3aii) with a smooth and dense surface. For the synthesized OCMC (Figure 3biii–bvi), the surface roughness of the polymer strand dropped slightly when the NaOH concentration increased from 30 to 70% as compared to the raw cellulose. This is due to the cellulose crystallinity being modified to allow mono-chloroacetate as an etherifying agent to access the cellulose molecule. Similar results were reported by Nur. et al. [36]. The cross-section of the CCMC film (Figure 3bi) revealed a smooth surface, whereas the cross-section of the OCMC film (Figure 3bii–bvi) experienced a rough surface that smoothed out as the concentration of NaOH increased up to 70%. For the following fabrication with the integration of BFO as a photocatalyst, the best CMC has generated at 60% NaOH concentration, which gave the highest DS. Figure 4a,b depicts a cross-section of the OCMC/BFO film which was observed by SEI to have a surface of CMC dispersed with BFO particles. The presence of BFO in CMC film was by the distribution of a white spot identified as a metal component of BiFeO_3 due to the greater atomic number of metals (Figure 4a), whilst the darker area was identified as the CMC membrane. The elemental mapping from the prepared OCMC/BFO film has been validated in Figure 4c–h. The result confirms that the BFO particles were homogeneously distributed in the OCMC membrane together with the spectrum and atomic weight composition. The presence of C, O, and Na was mainly from the CMC film where the Bi and Fe were dedicated to BFO confirmed from the EDS analysis.



(a)



(b)

Figure 3. SEM images $\times 2000$ of (i) cellulose at (ii) commercial CMC (iii) 20% NaOH (iv) 40% NaOH (v) 60% NaOH (vi) and 70% NaOH at $\times 2000$ (a); SEM images of cross-section of OCMC film at $\times 300$ for (i) CCMC (ii) 30% NaOH (iii) 40% NaOH (iv) 50% NaOH (v) 60% NaOH and (vi) 70% NaOH (b).

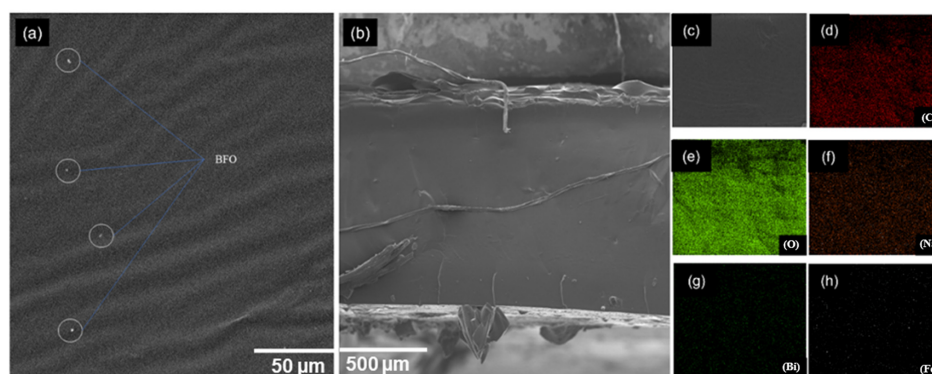


Figure 4. Electron backscattering SEM image (a) and cross-section OCMC/BFO film (b), mapping distribution of C, O, Na, Bi, Fe within the layer of $\text{CMC}_{\text{OPEFB}}/\text{BiFeO}_3$ film produced (c–h).

2.4. ATR-FTIR

FTIR study is also an optical analysis method used to understand the chemical composition of the prepared materials. The FTIR spectra obtained in the range between 4000 and 1000 cm^{-1} for the synthesized sample are displayed in Figure 5. The frequency of the absorption bands of cellulose and carboxymethyl cellulose from OPEFB (OCMC) obtained from various concentrations of NaOH and alkalization reaction time were similar, indicating that cellulose and commercial CMC have identical functional groups. In both cellulose and CMC, the peak found at 1030 cm^{-1} (Figure 5a) belongs to the (C–O–C stretching) ether groups. The new characteristic peak for OCMC at 1700 cm^{-1} (Figure 5a–c) corresponds to the (C=O stretching) group in the substituent group of OCMC products or some that comprise by-products, while the value of 1420 cm^{-1} relates to the carboxyl group as salts. The use of monochloroacetate in the etherification stage resulted in the carboxyl groups being substituted with carboxymethyl groups, resulting in the conversion of cellulose to CMC. The peak roughly at 3400 cm^{-1} suggests that the hydroxyl group is substituted during the etherification process (–OH stretching). Thus, comparisons of C=O and –OH peaks can be used to evaluate the extent of substitution (Figure 5c).

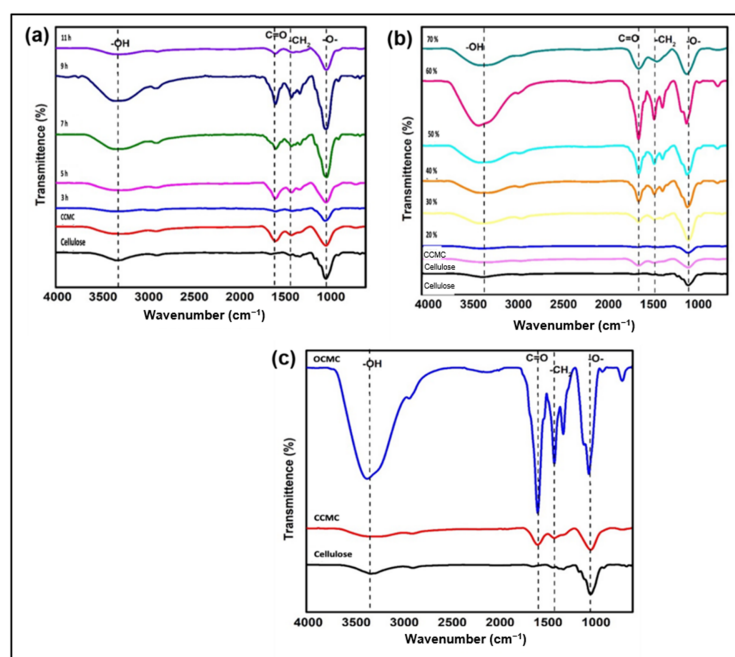


Figure 5. FTIR spectra of OCMC synthesized with various alkalization times (a); OCMC synthesized with various concentrations of NaOH solution (b); Comparison of cellulose, CCMC, and OCMC synthesized at 9 h with 60% NaOH solution (c).

2.5. X-Ray Diffraction (XRD) Analysis

An X-ray diffraction study was also performed on the prepared samples to analyze the crystalline nature of the product. The X-ray diffraction (XRD) pattern of CCMC and OCMC (using OCMC with 60% NaOH 9 h reaction time) films are shown in Figure 6. As for the CCMC, the diffraction peaks (dotted line) appeared at $2\theta = 23.46^\circ$ and 26.10° , indicating its semi-crystalline phase [37]. These findings demonstrate that OCMC was successfully synthesized as peaks similar to CCMC.

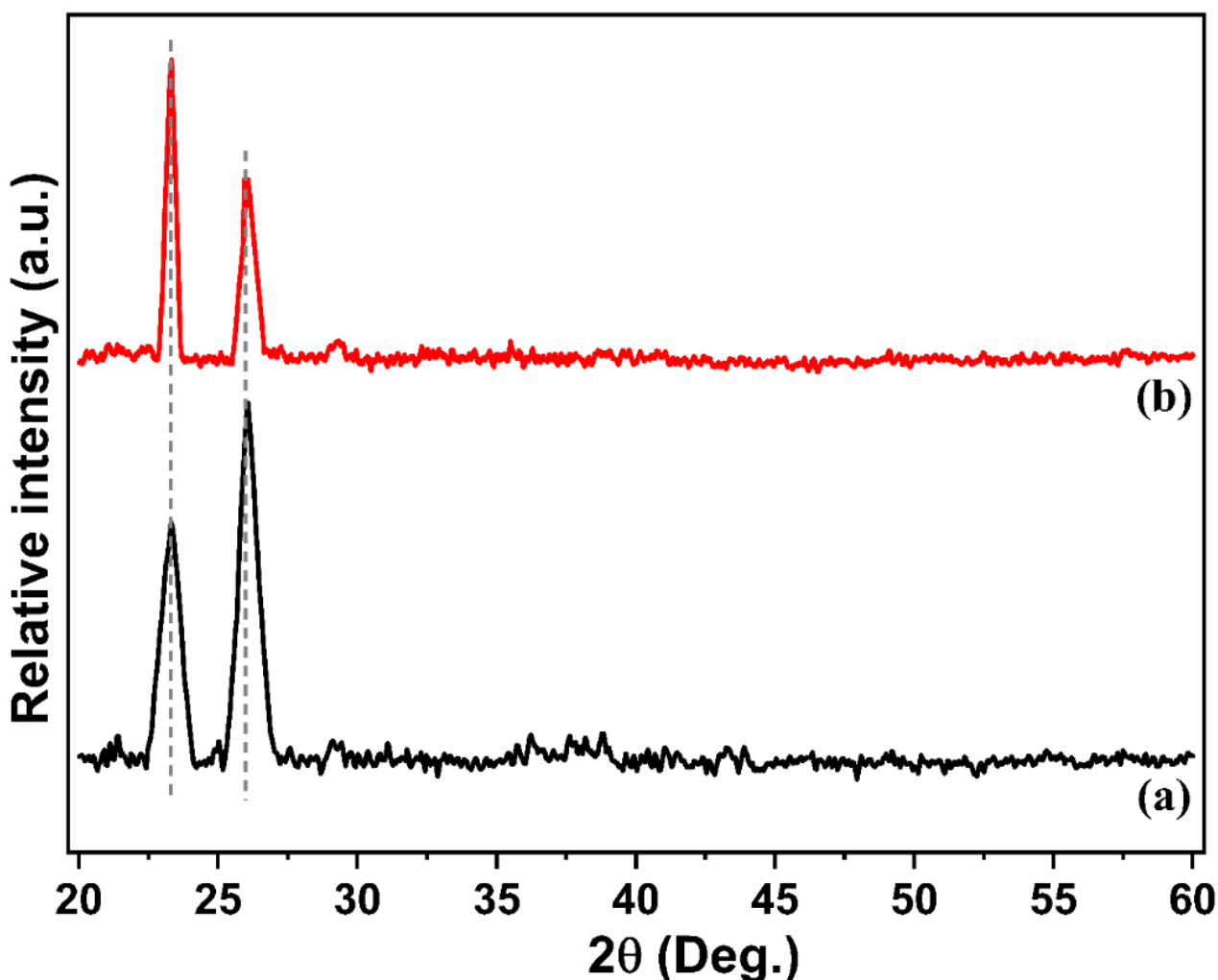


Figure 6. XRD pattern of film of CCMC (a) and OCMC (b).

2.6. Contact Angle and Tensile Strength Measurement

Contact angle measurement can be used to determine the hydrophilicity and hydrophobicity of CMC film as shown in Figure 7. It was notable that CMC produced with 20% NaOH was unable to be used for the preparation of the stable and intact film. The OCMC films prepared above 20% NaOH were considered hydrophilic films due to the value contact angle values less than 65° . CMC prepared with 60% NaOH concentration was excellent for future exploration since the value was the lowest. Table 1 summarized that CMC obtained with 60% NaOH concentration was ideal for further investigation, as the value was the lowest and closest to the CCMC (control), as shown in Figure 7.

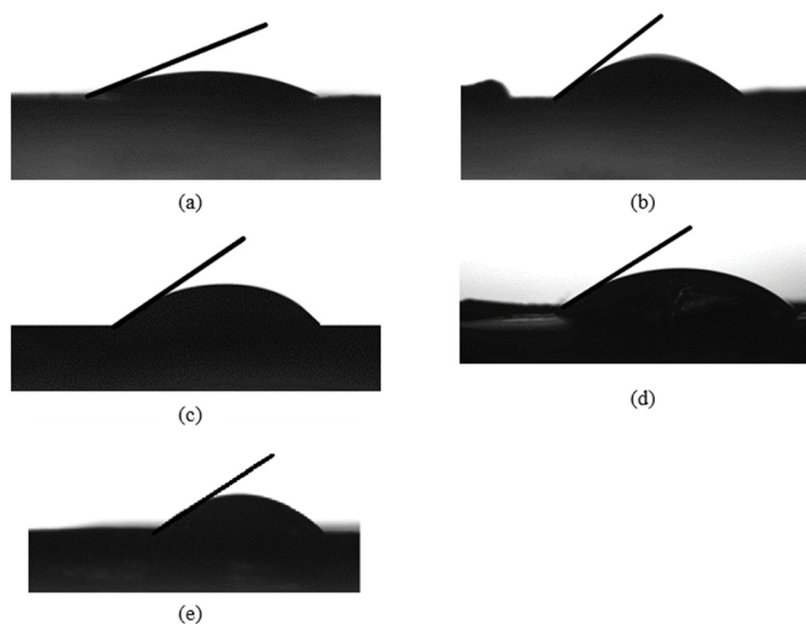


Figure 7. Contact angle images of CCMC film (a), OCMC film prepared with 40% (b), 50% (c), 60% (d) and 70% (e) NaOH within 3 h.

Table 1. Contact angle value of and tensile strength of CMC films produced from OPEFB at different NaOH concentrations within 3 h.

Film Sample	Contact Angle (°)	Tensile Strength (MPa)
CCMC	23.5 ± 1.04	0.31 ± 0.09
OCMC 30%	Not detected	3.54 ± 0.960
OCMC 40%	40.5 ± 1.72	3.54 ± 0.10
OCMC 50%	38.9 ± 0.45	0.29 ± 0.32
OCMC 60%	35.0 ± 0.10	0.11 ± 0.15
OCMC 70%	39.7 ± 0.36	0.15 ± 0.01

As shown in Table 1, the NaOH concentration influenced the tensile strength (TS) of OCMC films. At 30% and 40% NaOH, the maximum TS yield was obtained due to the non-elastic film formed during its formation. As NaOH concentrations of 50–60% were applied, TS of the resultant films was improved. Nevertheless, the TS of the OCMC films dropped to 60% NaOH concentration. The higher intermolecular forces between the polymer chains resulted in greater TS when more carboxymethyl groups related to the DS were present. The reduction of TS of OCMC films at higher concentrations of NaOH was observed to be due to sodium glycolate formation leading to polymer degradation. The increase in the formation of sodium glycolate reduced the CMC content and thus reduced intermolecular forces.

2.7. Optical Spectroscopy

The absorption spectra of BFO nanocomposites were shown in Figure 8a, while the Kubelka-Munk equation calculates the energy band gap for BFO nanocomposite films. From the plot observed in Figure 8b, extrapolation of the tangent line revealed that the band gap of BFO-integrated CCMC and OCMC was 2.04 eV and 2.15 eV, respectively. The direct band gap energy in this study agrees with the study reported [37]. The narrow band gap values of CCMC/BFO and OCMC/BFO composite films allow them to be used in visible light or direct sunlight. This feature is interesting, as when the samples are exposed to natural light, they will absorb a greater amount of sunlight to exert the photocatalytic activity due to their broader absorption spectrum.

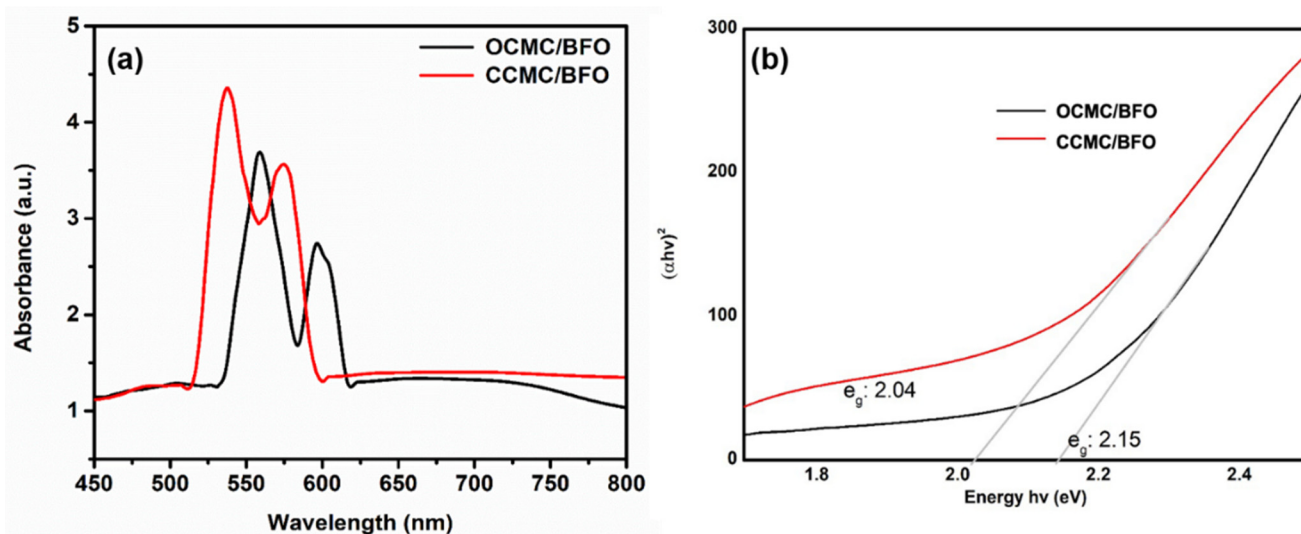


Figure 8. (a) UV-Vis spectra and (b) Band gap of CCMC/BFO and OCMC/BFO composite films.

2.8. Photocatalytic Degradation Efficiency

The preliminary study for the photocatalytic activity of commercial and synthesized BFO nanocomposite films was carried out for the degradation of 10 ppm of methyl orange (MO) and Congo red (CR) under direct sunlight. The efficiency removal for CCMC/BFO towards CR was enhanced to 95.49% after 3-h treatment, whereas a similar result was obtained in the case of OCMC/BiFeO₃ at 92.50%. Figure 9 indicated the removal efficiency towards MO by CCMC/BiFeO₃ has increased to 92.93% while that of synthesized OCMC/BFO composite film showed an increment of removal up to 89.56%. The results of photodegradation of synthesized OCMC/BFO composite film were comparable and as efficient as the CCMC. It is interesting to note that the stability and structure of OCMC/BFO films remained intact after 3 h of photocatalytic activity (Figure 9a,b towards CR and MO respectively, as compared to commercial CCMC/BFO film. Therefore, it can be concluded that the formation of CMC from waste solid OPEFB was highly stable compared to commercial CMC film (Figure 10). This benefit improves photocatalyst composite film separation after treatment and allows it to be reused for the next cycle.

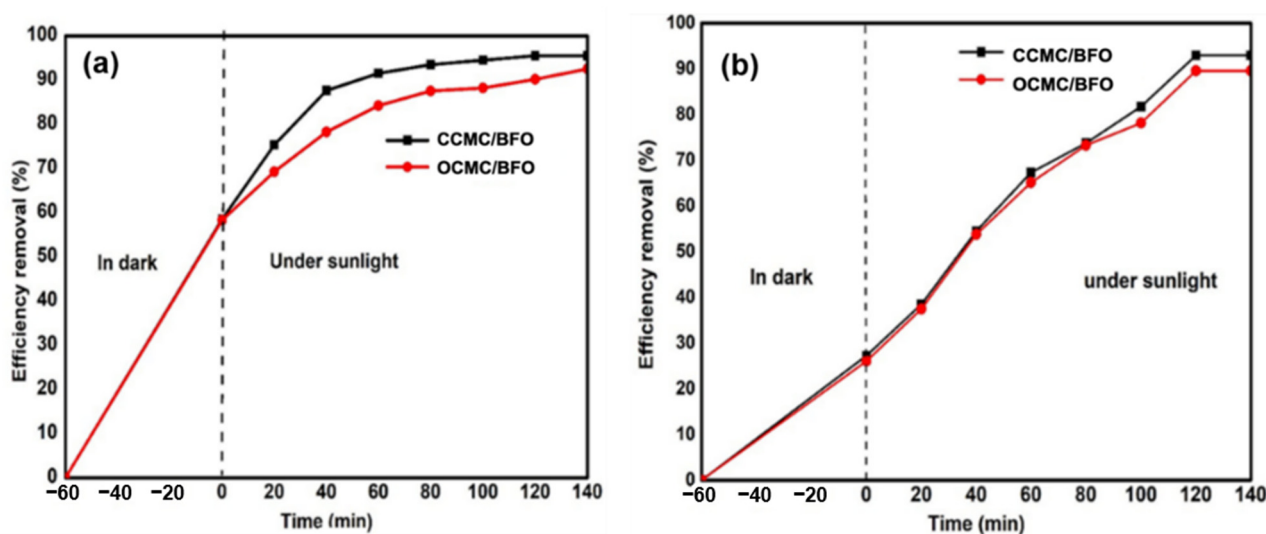


Figure 9. Efficiency removal of nanocomposite film CMC/BFO and CMC_{OPEFB}/BFO after a 3-h treatment, (a) CR, (b) MO.

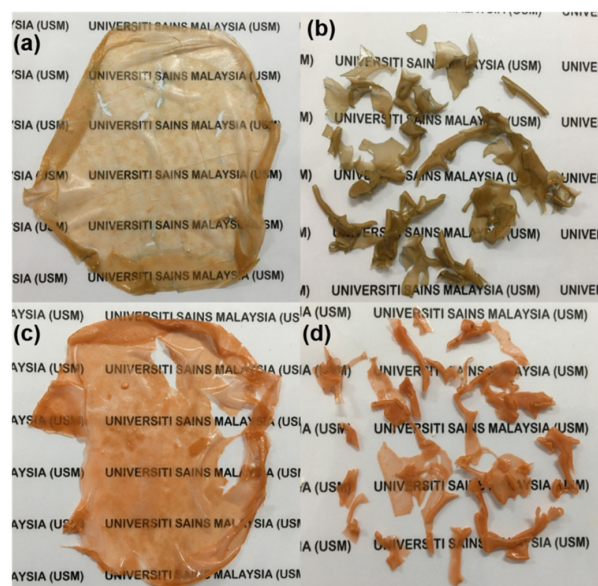


Figure 10. The stability of the film of CMC/BFO and CCMC/BFO films after 3-h treatment for 10 ppm of Congo red (a,b) and methyl orange (c,d).

The reusability was examined by repeatedly using the same hybrid film to degrade fresh dye solution under direct sunlight. Only OCMC composite BFO catalyst-loaded film was tested for the reusability experiment, since the CCMC composite is not stable after one cycle. After finishing each run of MO and CR dye photodegradation, the catalyst film was dried in air at room temperature for the next run. Figure 11 shows four runs of reusability experiments carried out with the same concentration of 10 ppm of both dyes for each test. The five consecutive runs were conducted without treatment to hybrid film except for drying before each test. The photocatalytic performance of hybrid films experienced a little change in degradation efficiency in the third to fifth cycles. It is important to note that a slower degradation with a low percentage happened after several cycles. This occurrence is related to the photodegradation rate on dye being slower due to the availability of active sites within the composite. The reusability experiment indicates that the OCMC-loaded BFO composite film is stable and reusable under direct sunlight irradiation.

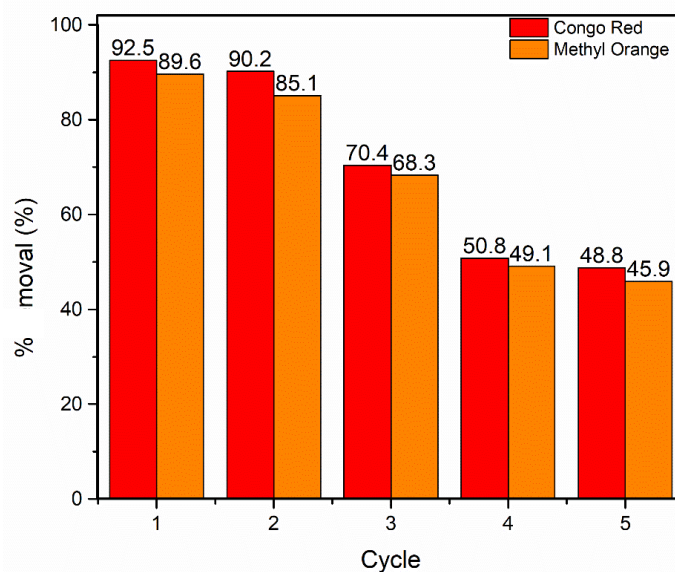


Figure 11. Reusability of the OCMC/BFO composite catalyst-loaded film for CR and MO dye photodegradation under direct sunlight irradiation.

3. Materials and Methods

3.1. Materials

Bismuth nitrate pentahydrate (98% purity) (Sigma-Aldrich, St. Louis, MO, United States), iron(III) nitrate nonahydrate (98% purity) (Sigma-Aldrich), κ-carrageenan (Sigma), ammonium persulphate (Sigma-Aldrich), oil palm empty fruit bunch, OPEFB raw fibre (courtesy gift from FSST, Universiti Kebangsaan Malaysia, Bangi, Malaysia), citric acid-1-hydrate (HmbG, Hamburg, Germany), carboxymethyl cellulose (Sigma), methyl orange dye (QReC, hydrochloric acid (HCl), and sodium hydroxide (NaOH). All the solutions were prepared using distilled water.

3.2. Methods

3.2.1. Extraction of Cellulose from OPEFB Pulp

It has been reported OPEFB consists of 27.3–65.0% cellulose, 13.50–33.8% hemicellulose and 14.1–31.16% lignin [38–40], which arranged in a complex hierarchical structure [41]. To isolate cellulose from OPEFB, alkali pre-treatment such as NaOH solution was used to eliminate the content of lignin, and the bleaching process was carried out in sodium chlorite solution. To remove the dust and contaminant, OPEFB was first washed with tap water, then soaked in water for 3 days and changed the water daily. Then, the OPEFB was dried for 3 days. The OPEFB was pulped from an oven-dry (OD) weight pulp using a twin digester with 26.0% sodium hydroxide (NaOH) solution (7:1 v/wt%) at 170 °C for 100 min. The pulp was then washed off with an excess amount of water to remove black liquor. The clean OPEFB was placed into the hydra pulper and was screened using a 15 mm long-flat screening for 10 min. After that, the prepared pulp was collected. To prepare cellulose, the obtained OPEFB pulp was bleached and then mercerized in an alkaline aqueous solution. In the bleaching step, 5 g of pulp were immersed in a mixed solution consisting of 1.5 g NaClO₂ in 160 mL distilled water and 10 drops of acetic acid (0.6 mL). The pulp was shaken upside down several times to ensure that the components were well-mixed. After that, the oxidizing was carried out at 75 °C. After 1 h, another 1.5 g NaClO₂ and 10 drops of acetic acid were added to the mixture. After 3 h, the product of oxidation was cooled and filtrated using Whatman filter paper. The residue was washed in an excess amount of distilled water till the pH to be neutral followed by acetone. The filter crucible with holocellulose is collected and stored for further process. Usually, holocellulose which has been separated still contains a small amount of lignin.

$$\text{Holocellulose composition (\%)} = \frac{\text{holocellulose weight}}{\text{weight of pulp (oven dried and extracted)}} \times 100\% \quad (1)$$

3.2.2. Cellulose Extraction Process from Holocellulose

The holocellulose crucible from the previous step will be processed using 17.5% of NaOH solution to extract cellulose in the water bath at 20 °C for 2 h. After that, the cellulose pulp content was filtered using the Buchner funnel fill with filter paper. The preparation procedure of cellulose isolated from OPEFB was shown in Figure 12a. Cellulose from OPEFB was converted into CMC via alkalization and carboxymethylation under heterogeneous conditions. About 5 g of cellulose was added into a three-neck round bottom flask. Then, 10 mL of various concentrations of NaOH aqueous solution (20, 30, 40, 50, 60, and 70%) were added and mechanically stirred at different durations such as 3, 5, 7, 9, and 11 h. After the alkalization treatment, the carboxymethylation process was conducted by adding 6.0 g of monochloroacetate (MCA) in 25 mL isopropanol, where the temperature was raised to 45 °C, and the reaction continued for 3 h. The mixture was then filtered and suspended in 300 mL of methanol overnight. The solution was neutralized with glacial acetic acid. The final product was purified by 70% ethanol, followed by 99.7% ethanol, three times to eliminate the undesirable by-products. The CMC obtained yield (128%) was dried at 60 °C before further use.

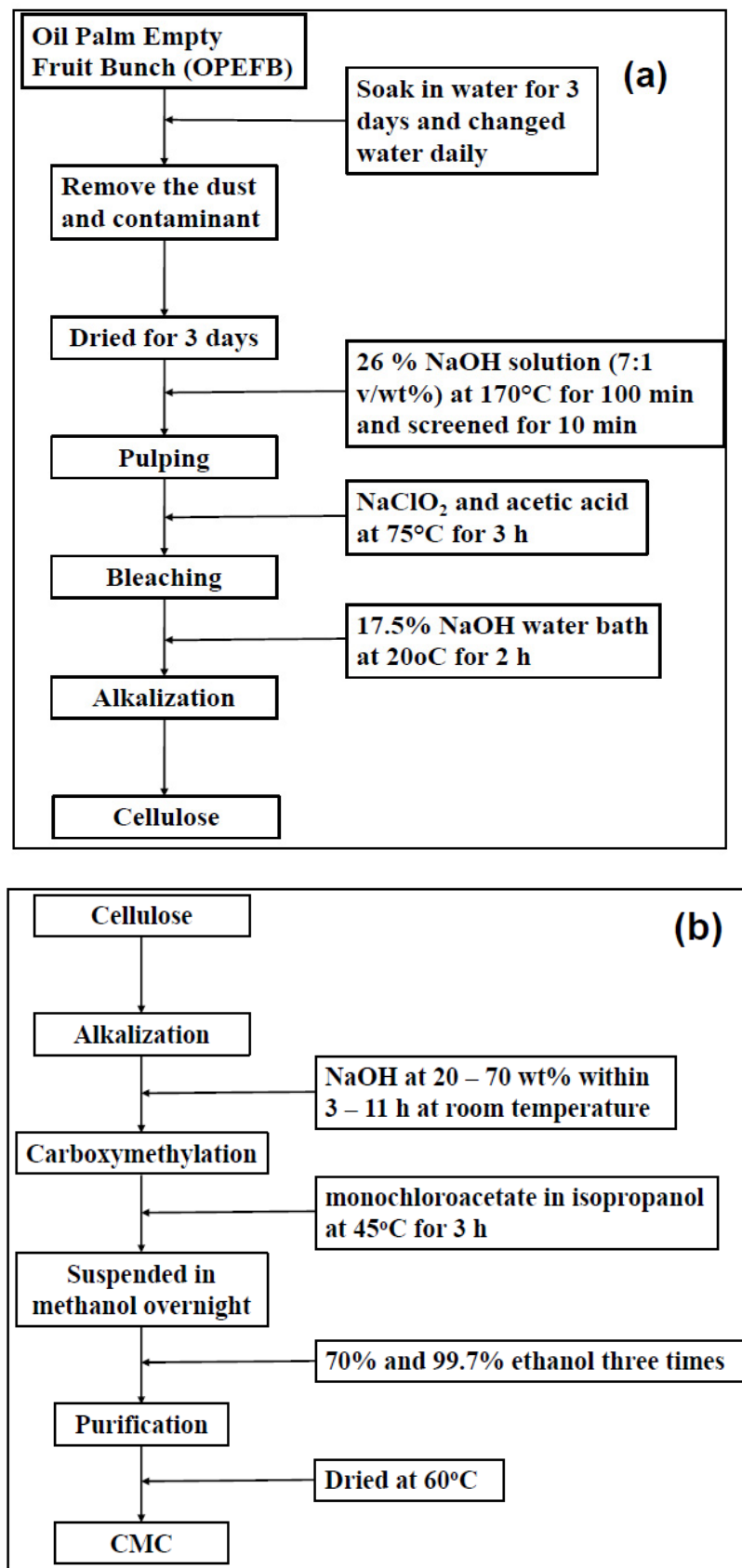


Figure 12. Preparation procedure of cellulose from OPEFB (a) and CMC from the extracted cellulose (b).

3.2.3. Determination of Degree of Substitution (DS) of CMC

The DS of the carboxylic group in CMC is the average number of the hydroxyl groups in the cellulose structure, which was substituted by carboxymethyl groups C-2, C-3 and C-6. Here, 1 g CMC was added to 50 mL of 95% ethanol, and 5 mL of 2 M nitric acid was added. The mixture was continuously stirred at room temperature and heated when stirred for 20 min. The solution was left to settle, and the residue was filtered and washed with 100 mL of 95% ethanol. The final product was dried in an oven for 3 h at 105 °C. CMC was added to 100 mL of distilled water while stirred 25 mL of 0.5 M NaOH was added and boiled for 20 min. The solution was titrated with 0.3 M HCl using phenolphthalein as an indicator. The titration was ended as the color changed from dark pink to colorless. The DS of CMC was calculated based on the equations below:

$$\text{Degree of substitution} = \frac{0.162 \times A}{1 - (0.058 \times A)} \quad (2)$$

$$A = \frac{BC - DE}{F} \quad (3)$$

where,

A = milli-equivalents of consumed acid per gram of specimen;

B = volume of NaOH added;

C = concentration of NaOH added;

D = volume of consumed HCl;

E = concentration of HCl used;

F = specimen grams used; 162 are the molecular weight of the anhydrous glucose unit, and 58 is the net increase in the anhydrous glucose unit for each substituted carboxymethyl group.

3.2.4. Preparation of CMC and CMC/BiFeO₃ Composites Film

For the fabrication of CMC polymer film, 1.25 g of CMC produced from OPEFB (OCMC) and commercial product (CCMC) were dissolved in 19 mL of distilled water and stirred for 3 h. After obtaining a homogeneous solution, a film was formed on glass plates (90 mm × 15 mm) by casting and then dried at 60 °C within 24 h. In the case of CMC/BiFeO₃ composite film, about 1.25 g of OCMC/CCMC was added into 0.6 mL of 1.04 M of citric acid under constant stirring. Next, 0.01 g of BFO was added to the mixture and continuously stirred for another 2 h to become a homogenous solution. The well-mixed solution was finally poured into a petri dish and kept for 24 h to obtain a nanocomposite film from CMC/BiFeO₃.

3.2.5. Characterization

Fourier transform infrared (FT-IR) spectra were collected using ATR-FTIR (Agilent, Beijing, China). The spectra were measured in the transmittance mode from an accumulation of 16 scans at a 16 cm⁻¹ resolution over the 4000–600 cm⁻¹ range. An X-ray diffractometer (Rigaku, Tokyo, Japan) was used to obtain X-ray diffraction patterns of CMC. Samples are prepared by pressing the powders between two glass slides into a flattened sheet. X-ray patterns are taken using radiation source Cu K α by supplying 40 kV and 40 mA to the X-ray generator. Patterns are recorded at 2 θ from 20° to 60°. The surface morphologies by FESEM (PhotoMetrics, Huntington Beach, CA, USA) were examined. Samples were coated with a thin layer of conducting material (platinum) and imaged at $\times 2000$ magnifications with 10–15 kV accelerating voltage. A focused, high-energy beam of the electron will interact with the surface of the sample and generate secondary electrons, backscattered electrons, and characteristic X-ray signals. The detector will perceive these signals, and images will be displayed on the cathode ray tube screen. The contact angle (θ) of water on film surfaces is measured using a contact angle analyzer with a 6 μm drop of distilled water on the surface of a film sample with dimensions 2.0 cm × 2.0 cm. The

measurement of electronic absorption spectra by using diffuse reflectance spectroscopy was done with a UV-Vis spectrophotometer (LAMBDA 25, Cartoni, Rome, Italy). The films were cut as required and screened using a Universal Testing Machine (Instron 5567) using a 500 N load cell at a speed of 5.0 mm/min. Film thickness was limited to 0.05–0.20 mm. For each sample, three readings have been recorded.

3.2.6. Photocatalytic Measurement

This test is based on the photodegradation of organic dyes, by the heterogeneous photocatalysis process. The MO and CR dyes were used as pollutant models. The photocatalytic behaviour of the synthesized samples was evaluated by examining the MO and CR degradation efficiency under sunlight radiation. The suspensions were magnetically stirred for 30 min continuously before light irradiation. After mixing, the suspension was exposed to sunlight irradiation under standard ambient conditions. The photocatalytic degradation was carried out under sunlight irradiation for 3 h and the aliquot was collected at the first hour and followed by every 20 min interval. The removal of MO and CR were observed at the wavelengths of 464 nm and 497 nm respectively. The absorbances of the dyes used as a model of pollutants during the photocatalytic activity tests were determined in a spectrophotometer (LAMBDA 25). The percentages of removal efficiency of MO and CR were then calculated using this Equation (4) [38]:

$$\text{Percentage of removal efficiency (\%)} = \left(1 - \frac{C_f}{C_o}\right) \times 100\% \quad (4)$$

where C_f = final concentration of dye (ppm); C_o = initial concentration of dye (ppm).

4. Conclusions

In summary, Bismuth ferrite (BiFeO_3) nanoparticles combined with carboxymethyl cellulose (CMC) are obtained from oil palm empty fruit bunch waste (OCMC). The presence of C, O, and Na was primarily from the CMC film, while the presence of Bi and Fe are confirmed by EDS analysis. From FTIR spectra, the peak at 1030 cm^{-1} in both cellulose and CMC belongs to the (C-O-C stretching) ether groups. The XRD pattern of CCMC and OCMC films indicates that they are semi-crystalline. The optical band gap of BFO-integrated CCMC and OCMC was found to be 2.04 eV and 2.15 eV, respectively. Further, The MO and CR dyes were used as pollutant models. The photocatalytic behavior of the synthesized samples was evaluated by examining the MO and CR degradation efficiency under sunlight radiation. Among all investigated samples, the maximum degree of substitution of 1.562 was found with 60% NaOH and 9 h of alkalization for the synthesized composite. The efficiency removal for CCMC/BFO towards CR was enhanced to 95.49% after 3-h treatment, whereas a similar result was obtained in the case of OCMC/ BiFeO_3 at 92.50%. In comparison to CCMC/BFO, the OCMC/BFO nanocomposite film was inherently stable after 3 h of photocatalytic treatment. In essence, this study provides a new finding that OCMC has a greater potential to be developed as embedded matrices for photocatalysts in environmental remediation, with highly durable operation in practical application.

Author Contributions: Conceptualization, S.A.H.M.A. and N.H.M.K.; data curation, I.A. and M.H.M.K.; formal analysis, S.A.H.M.A., I.A., M.H.M.K., S.S.I., K.D.N. and N.H.M.K.; investigation, S.A.H.M.A., S.S.I., K.D.N. and N.H.M.K.; methodology, S.A.H.M.A., K.D.N. and N.H.M.K.; validation, S.S., I.A., M.H.M.K., S.S.I. and K.D.N.; visualization, S.S., I.A. and M.H.M.K.; writing—original draft, N.H.M.K.; writing—review & editing, S.S. All authors have read and agreed to the published version of the manuscript.

Funding: The author gratefully acknowledges financial assistance from the Ministry of Higher Education (MOHE) under the Fundamental Research Grant Scheme (FRGS) [FRGS/1/2019/STG07/USM/02/7/], USM Bridging grant [304/PKIMIA/6316050] and Van Lang University for their financial support.

Data Availability Statement: Not applicable.

Acknowledgments: The author also acknowledges School of Chemical Sciences, Center for Global Archeological Research, and School of Technological Industry, USM for the research facilities.

Conflicts of Interest: The authors declare no conflict of interest.

References

1. Badvi, K.; Javanbakht, V. Enhanced photocatalytic degradation of dye contaminants with TiO₂ immobilized on ZSM-5 zeolite modified with nickel nanoparticles. *J. Clean. Prod.* **2021**, *280*, 124518. [[CrossRef](#)]
2. Bansal, P.; Sud, D. Photodegradation of commercial dye, Procion Blue HERD from real textile wastewater using nanocatalysts. *Desalination* **2011**, *267*, 244–249. [[CrossRef](#)]
3. Zouhier, M.; Tanji, K.; Navio, J.A.; Hidalgo, M.C.; Jaramillo-Páez, C.; Kherbeche, A. Preparation of ZnFe₂O₄/ZnO composite: Effect of operational parameters for photocatalytic degradation of dyes under UV and visible illumination. *J. Photochem. Photobiol. a-Chem.* **2020**, *390*, 112305. [[CrossRef](#)]
4. Mittal, H.; Khanuja, M. Hydrothermal in-situ synthesis of MoSe₂-polypyrrole nanocomposite for efficient photocatalytic degradation of dyes under dark and visible light irradiation. *Sep. Purif. Technol.* **2021**, *254*, 117508. [[CrossRef](#)]
5. Abdelrahman, E.A.; Hegazey, R.; Kotp, Y.H.; Alharbi, A. Facile synthesis of Fe₂O₃ nanoparticles from Egyptian insecticide cans for efficient photocatalytic degradation of methylene blue and crystal violet dyes. *Spectroc. Acta A Mol Bio. Spectr.* **2019**, *222*, 117195. [[CrossRef](#)]
6. Ehsan, M.F.; Bashir, S.; Hamid, S.; Zia, A.; Abbas, Y.; Umbreen, K.; Ashiq, M.N.; Shah, A. One-pot facile synthesis of the ZnO/ZnSe heterostructures for efficient photocatalytic degradation of azo dye. *Appl. Surf. Sci.* **2018**, *459*, 194–200. [[CrossRef](#)]
7. Hien, N.; Nguyen, L.H.; Van, H.T.; Nguyen, T.D.; Chu, T.H.H.; Nguyen, T.V.; Trinh, V.T.; Vu, X.H.; Aziz, K.H.H. Heterogeneous catalyst ozonation of Direct Black 22 from aqueous solution in the presence of metal slags originating from industrial solid wastes. *Sep. Purif. Technol.* **2020**, *233*, 115961. [[CrossRef](#)]
8. Aziz, K.H.H.; Mahyar, A.; Miessner, H.; Mueller, S.; Kalass, D.; Moeller, D.; Khorshid, I.; Rashid, M.A.M. Application of a planar falling film reactor for decomposition and mineralization of methylene blue in the aqueous media via ozonation, Fenton, photocatalysis and non-thermal plasma: A comparative study. *Process Saf. Environ. Prot.* **2018**, *113*, 319–329. [[CrossRef](#)]
9. Karim, M.A.H.; Aziz, K.H.H.; Omer, K.M.; Salih, Y.M.; Mustafa, F.; Rahman, K.O.; Mohammad, Y. Degradation of aqueous organic dye pollutants by heterogeneous photo-assisted Fenton-like process using natural mineral activator: Parameter optimization and degradation kinetics. *IOP Conf. Ser. Earth Environ. Sci.* **2021**, *958*, 012011. [[CrossRef](#)]
10. Ibhaddon, A.O.; Fitzpatrick, P. Heterogeneous Photocatalysis: Recent Advances and Applications. *Catalysts* **2013**, *3*, 189–218. [[CrossRef](#)]
11. Gao, F.; Chen, X.Y.; Yin, K.B.; Dong, S.; Ren, Z.F.; Yuan, F.; Yu, T.; Zou, Z.G.; Liu, J.-M. Visible-light photocatalytic properties of weak magnetic BiFeO₃ nanoparticles. *Adv. Mater.* **2007**, *19*, 2889–2892. [[CrossRef](#)]
12. Deng, J.; Banerjee, S.; Mohapatra, S.K.; Smith, Y.R.; Misra, M. Bismuth iron oxide nanoparticles as photocatalyst for solar hydrogen generation from water. *J. Fundam. Renew. Energy Appl.* **2011**, *1*, R101204. [[CrossRef](#)]
13. Vasudevan, R.K.; Liu, Y.; Li, J.; Liang, W.-I.; Kumar, A.; Jesse, S.; Chen, Y.-C.; Chu, Y.-H.; Nagarajan, V.; Kalinin, S.V. Nanoscale Control of Phase Variants in Strain-Engineered BiFeO₃. *Nano Lett.* **2011**, *11*, 3346–3354. [[CrossRef](#)] [[PubMed](#)]
14. Megashah, L.N.; Ariffin, H.; Zakaria, M.R.; Hassan, M.A. Multi-step pretreatment as an eco-efficient pretreatment method for the production of cellulose nanofiber from oil palm empty fruit bunch. *Asia Pac. J. Mol. Biol. Biotechnol.* **2018**, *26*, 1–8. [[CrossRef](#)]
15. Hassan, M.A.; Abd-Aziz, S. *23-Waste and Environmental Management in the Malaysian Palm Oil Industry, in Palm Oil*; Lai, O.-M., Tan, C.-P., Akoh, C.C., Eds.; AOCS Press: Urbana, IL, USA, 2012; pp. 693–711.
16. Shuit, S.H.; Tan, K.T.; Lee, K.T.; Kamaruddin, A.H. Oil palm biomass as a sustainable energy source: A Malaysian case study. *Energy* **2009**, *34*, 1225–1235. [[CrossRef](#)]
17. Qi, X.; Tong, X.; Pan, W.; Zeng, Q.; You, S.; Shen, J. Recent advances in polysaccharide-based adsorbents for wastewater treatment. *J. Clean. Prod.* **2021**, *315*, 128221. [[CrossRef](#)]
18. Rachtanapun, P.; Luangkamin, S.; Tanprasert, K.; Suriyatem, R. Carboxymethyl cellulose film from durian rind. *LWT Food Sci. Technol.* **2012**, *48*, 52–58. [[CrossRef](#)]
19. Pinto, E.; Aggrey, W.N.; Boakye, P.; Amenuvor, G.; Sokama-Neuyam, Y.A.; Fokuo, M.K.; Karimaie, H.; Sarkodie, K.; Adenutsi, C.D.; Erzuah, S.; et al. Cellulose processing from biomass and its derivatization into carboxymethylcellulose: A review. *Sci. Afr.* **2022**, *15*, e01078. [[CrossRef](#)]
20. Huang, C.M.; Chia, P.X.; Lim, C.S.S.; Nai, J.Q. Synthesis and characterisation of carboxymethyl cellulose from various agricultural wastes. *Cellul. Chem. Technol.* **2017**, *51*, 665–672.
21. Asl, S.A.; Mousavi, M.; Labbafi, M. Synthesis and characterization of carboxymethyl cellulose from sugarcane bagasse. *J. Food Processing Technol.* **2017**, *8*, 687.
22. Shui, T.; Feng, S.; Chen, G.; Li, A.; Yuan, Z.; Shui, H.; Kuboki, T.; Xu, C. Synthesis of sodium carboxymethyl cellulose using bleached crude cellulose fractionated from cornstalk. *Biomass Bioenergy* **2017**, *105*, 51–58. [[CrossRef](#)]
23. Waring, M.J.; Parsons, D. Physico-chemical characterisation of carboxymethylated spun cellulose fibres. *Biomaterials* **2001**, *22*, 903–912. [[CrossRef](#)]

24. Toğrul, H.; Arslan, N. Production of carboxymethyl cellulose from sugar beet pulp cellulose and rheological behaviour of carboxymethyl cellulose. *Carbohydr. Polym.* **2003**, *54*, 73–82. [[CrossRef](#)]
25. Pushpamalar, V.; Langford, S.; Ahmad, M.; Lim, Y. Optimization of reaction conditions for preparing carboxymethyl cellulose from sago waste. *Carbohydr. Polym.* **2006**, *64*, 312–318. [[CrossRef](#)]
26. Yeasmin, M.S.; Mondal, M.I.H. Synthesis of highly substituted carboxymethyl cellulose depending on cellulose particle size. *Int. J. Biol. Macromol.* **2015**, *80*, 725–731. [[CrossRef](#)]
27. Gatot, S.H.; Djagal, W.M.; Sri, A. Synthesis and characterization of sodium carboxymethylcellulose from pod husk of Cacao (*Theobroma cacao* L.). *Afr. J. Food Sci.* **2012**, *6*, 180–185.
28. Rachtanapun, P.; Jantrawut, P.; Klunklin, W.; Jantanasakulwong, K.; Phimolsiripol, Y.; Leksawasdi, N.; Seesuriyachan, P.; Chaiyaso, T.; Insomphun, C.; Phongthai, S.; et al. Carboxymethyl Bacterial Cellulose from Nata de Coco: Effects of NaOH. *Polymers* **2021**, *13*, 348. [[CrossRef](#)] [[PubMed](#)]
29. Bono, A.; Ying, P.H.; Yan, F.Y.; Muei, C.L.; Sarbatly, R.; Krishnaiah, D. Synthesis and characterization of carboxymethyl cellulose from palm kernel cake. *Adv. Nat. Appl. Sci.* **2009**, *3*, 5–12.
30. Jia, F.; Liu, H.-J.; Zhang, G.-G. Preparation of Carboxymethyl Cellulose from Corncob. *Procedia Environ. Sci.* **2016**, *31*, 98–102. [[CrossRef](#)]
31. Rasid, N.S.A.B.; Zainol, M.M.; Amin, N.A.S. Synthesis and Characterization of Carboxymethyl Cellulose Derived from Empty Fruit Bunch. *Sains Malays.* **2021**, *50*, 2523–2535. [[CrossRef](#)]
32. Febriani, S.N.M.; Junaedi, A.B. Preparation of carboxymethyl cellulose produced from Purun Tikus (*Eleocharis Dulcis*). In *AIP Conference Proceedings, Yogyakarta, Indonesia, 15–16 May 2017*; AIP Publishing LLC: Melville, NY, USA, 2017.
33. Parid, D.M.; Rahman, N.A.A.; Baharuddin, A.S.; Mohammed, M.A.P.; Johari, A.M.; Razak, S.Z.A. Synthesis and Characterization of Carboxymethyl Cellulose from Oil Palm Empty Fruit Bunch Stalk Fibres. *BioResources* **2017**, *13*, 535–554.
34. Zhao, H.; Cheng, F.; Li, G.; Zhang, J. Optimization of a process for carboxymethyl cellulose (CMC) preparation in mixed solvents. *Int. J. Polym. Mater. Polym. Biomater.* **2003**, *52*, 749–759. [[CrossRef](#)]
35. Casaburi, A.; Rojo, M.; Cerrutti, P.; Vázquez, A.; Foresti, M.L. Carboxymethyl cellulose with tailored degree of substitution obtained from bacterial cellulose. *Food Hydrocoll.* **2018**, *75*, 147–156. [[CrossRef](#)]
36. Mohamood, N.F.A.-Z.T.; Halim, A.H.A.; Zainuddin, N. Carboxymethyl Cellulose Hydrogel from Biomass Waste of Oil Palm Empty Fruit Bunch Using Calcium Chloride as Crosslinking Agent. *Polymers* **2021**, *13*, 4056. [[CrossRef](#)] [[PubMed](#)]
37. Zaahari, N.A.A.; Malaysia, M.U.S.; Huat, T.L.; Kaus, N.H.M.; Kassim, M.H.M.; Othman, M.Z. Remarkable Catalytic Activity of CMC/BiFeO₃ Nanocomposite Film for the Degradation of Methyl Orange Under Direct Sunlight Radiation. *J. Phys. Sci.* **2019**, *30*, 23–40. [[CrossRef](#)]
38. Yiin, C.L.; Ho, S.; Yusup, S.; Quitain, A.T.; Chan, Y.H.; Loy, A.C.M.; Gwee, Y.L. Recovery of cellulose fibers from oil palm empty fruit bunch for pulp and paper using green delignification approach. *Bioresour. Technol.* **2019**, *290*, 121797. [[CrossRef](#)]
39. Sudiyani, Y.; Styarini, D.; Triwahyuni, E.; Sudiarmanto; Sembiring, K.C.; Aristiawan, Y.; Abimanyu, H.; Han, M.H. Utilization of Biomass Waste Empty Fruit Bunch Fiber of Palm Oil for Bioethanol Production Using Pilot-Scale Unit. *Energy Procedia* **2013**, *32*, 31–38. [[CrossRef](#)]
40. Isroi; Cifriadi, A.; Panji, T.; Wibowo, N.A.; Syamsu, K. Bioplastic production from cellulose of oil palm empty fruit bunch. *IOP Conf. Ser. Earth Environ. Sci.* **2017**, *65*, 012011. [[CrossRef](#)]
41. Norrrahim, M.N.F.; Ariffin, H.; Yasim-Anuar, T.A.T.; Ghaemi, F.; Hassan, M.A.; Ibrahim, N.A.; Ngee, J.L.H.; Yunus, W.M.Z.W. Superheated steam pretreatment of cellulose affects its electrospinnability for microfibrillated cellulose production. *Cellulose* **2018**, *25*, 3853–3859. [[CrossRef](#)]